PAPER

Check for updates

Preparation and photocatalytic application of a S, Nd double doped nano-TiO₂ photocatalyst†

Shuo Wang, ID * Liming Bai and Xinling Ao

Nowadays, water pollution is getting more and more severe in society, and recently the rational use of photocatalytic technology to treat sewage has become a hot spot for research. Because of the low-cost and environmental friendliness of nano-TiO₂, it has attracted widespread attention. In this paper, we dope sulfur and neodymium into nano-titanium dioxide *via* a sol–gel method. The synthesized S, Nd-codoped-TiO₂ was characterized *via* transmission electron microscopy, scanning electron microscopy, X-ray diffraction, X-ray photoelectron spectroscopy, EDS and N_2 adsorption–desorption isotherms. Then the real-life dye reactive red (X-3B) was used as the target degradant to compare the levels of practicality of single-doped and double-doped photocatalysts. The results showed that the photocatalytic activity of S, Nd-codoped-TiO₂ was significantly higher than that of Nd–TiO₂. The double-doped photocatalyst was transformed from anatase to rutile, and the bandgap was reduced considerably. The responding ability to visible light also increased, so S, Nd-codoped-TiO₂ has obvious advantages and has better degradation efficiency for the target degradation products. Under xenon lamp irradiation and pH = 4 conditions, the degradation of reactive red using the new catalyst reached 93.2%. The new catalyst has high practicality and also indicates a new direction for wastewater treatment.

1. Introduction

With the rapid development of the dying and weaving industries, dye wastewater has become one of the most challenging problems for human beings. Traditional sewage treatment mainly includes physical degradation, chemical degradation, and biodegradation. However, these methods are time-consuming and consume much energy. The discovery of photocatalytic technology has completely altered the dilemma of disposing of dye wastewater and has made a difference in the protection of human water resources.[1–8]

Since the innovation of photocatalytic technology in 1972, public interest in photocatalysis has continued unabated.[9] With the deepening of research, photocatalysis technology can not only produce hydrogen, but also effectively degrade water pollution. This brings benefits to societies with serious water pollution. In photocatalyst experiments applied to water pollution degradation, TiO₂ is the most widely used compound. This is because TiO₂ has the advantages of low cost, low toxicity, and excellent chemical stability.[10–14] When light is incident on the semiconductor TiO₂, if the energy of the photon generated by the light is higher than the band gap level of the semiconductor TiO₂, an electron is excited from the valence band to the

conduction band. However, the photocatalytic performance of TiO₂ is poor due to the extremely short recombination time of photogenerated electrons and electron holes. Therefore, prolonging the photogenerated electron and hole recombination time has become a hot spot in research into TiO₂ photocatalysts. Due to the wide bandgap of TiO₂ (E_g = 3.2 eV), it can only be excited by ultraviolet radiation at a wavelength of 387 nm; it can also agglomerate easily with poor dispersion and has a low utilization rate for sunlight. Therefore, researchers have adopted modified or retouched TiO₂ to improve defects and improve photocatalytic efficiency.[15–20] In 2017, Balter Trujillo-Navarrete *et al.* explained the reasons for lattice distortion caused by Nd–TiO₂, which affects the recombination rate of photoelectrons and holes and improves photocatalytic performance.[21] In 2018, Thirupathi Boningari used a one-step method to synthesize S–TiO₂ and confirmed that S doping could effectively reduce the optical band gap of TiO₂. The photoresponsive wavelength of TiO₂ can not only be extended beyond the visible region, but also the absorption of light in the ultraviolet region can be maintained.[22] However, many experiments have confirmed that the single doping of TiO₂ does not completely increase the utilization of titanium dioxide. Therefore, double-doped photocatalysts and multi-doped photocatalysts have become hot spots for research.[23–25] A large number of studies have found that the rare earth element neodymium is more active in terms of chemical properties, cheaper and more readily available, and can be well combined with titanium dioxide, so it has attracted the attention of

College of Chemistry and Chemical Engineering, Qiqihar University, Qiqihar, Heilongjiang, 161006, P. R. China. E-mail: 345508266@qq.com; Tel: +86 15561926110

scholars. The contribution of non-metallic sulfur to the light absorption capacity of titanium dioxide is well known, so combining the advantages of both would be a very meaningful exercise.

Based on these analyses, we first prepared a single-doped photocatalyst $Nd–TiO_2$ with a low electron–hole recombination rate using a sol–gel method. Then, adopting the same process, Nd and S are co-doped into the TiO_2 structure to obtain a bifunctional catalyst with a low electron recombination rate and wide photoresponse range. The S element is doped while controlling the Nd content. The purpose of doing this is to obtain photocatalysts with two advantages. Degradation using $Nd–TiO_2$ and S, Nd-codoped-TiO_2 photocatalysts with diverse contents were investigated using active red as the target degradation product. The results are positive. The double-doped photocatalyst has significantly higher photo-degradation capability than the single-doped photocatalyst, and the double-doped photocatalyst has a broader light response range. This research has provided valuable theoretical exploration of and technical support for the large-scale treatment of dye wastewater.

2.   Experimental

2.1   Reagents and apparatus

Thiourea, tetrabutyl titanate and neodymium nitrate were purchased from Tianjin Fuchen Reagent Factory of China. Reactive red was a product of Tianjin Kaitong Reagent Factory of China. All reagents were commercially available and were not subjected to secondary purification. Infrared spectroscopy was performed using a Perkin Elmer Nicolet-50X FTIR spectrometer (JEOL Ltd., Japan). X-ray diffraction analysis was performed using a Dmax-IIIC X-ray diffractometer (JEOL Ltd., Japan). Structural analysis was performed using a S-4300 field emission scanning electron microscope and a H7650 transmission electron microscope (HITACHI Ltd., Japan). UV-visible spectra of the samples were recorded on a UV-visible DRS instrument (DRS; UV-2450, Shimadzu Co.) using $BaSO_4$ as the standard reference. Adsorption/desorption analysis was performed using an Autosorb 1 physical adsorption–desorption instrument (QUANTACHROME Ltd., America). XRD analysis was performed using a D8 Focus X-ray powder diffractometer (German Bruker-Axs). The sample was fluorescently characterized using an F-4500 fluorescence spectrophotometer, manufactured by Hitachi, Japan. All pH values were measured using a pH indicator manufactured by Beijing Sartorius.

2.2   The preparation of S, Nd–TiO₂

Tetrabutyl titanate (25 mL) and glacial acetic acid (4 mL) were dissolved in 34 mL of anhydrous ethanol, and this mixture was stirred continuously for 30 minutes. The pH of the solution was then adjusted using dilute hydrochloric acid solution. The pH of the mixture was adjusted to 3. The resulting mixture was placed in an ultrasonic bath and irradiated for 10 minutes under a sound wave of 40 kHz to make the mixing more uniform. Four portions of weighed neodymium nitrate (0.166 g

each) were added to distilled water (4 mL) and anhydrous ethanol (17 mL), then thiourea (0 g, 0.170 g, 0.340 g or 0.51 g) was added. Then the pH was adjusted to 3 with an aqueous solution of hydrochloric acid. The mixture was sonicated at the same intensity. Under magnetic stirring, the neodymium nitrate mixture was added dropwise to the tetrabutyl titanate solution at 1–2 drops per second. After magnetic stirring for 10 h, it was let stand for 10 h. The mixture was then placed in a drying oven at 70 °C and dried for 2 h, then it was moved into a muffle furnace and calcined for 2 h (450 °C). Based on the above method, we synthesized photocatalysts with different S content values.

2.3   Photocatalytic activity tests

The photocatalytic activities of the S, Nd–TiO₂ nanocomposites were evaluated by measuring the absorbance of reactive red solution added to the photocatalysts under sunlight irradiation. In the experiment, the light source was condensed under a cylindrical glass cannula, and each of the outer tubes contained 50 mL of reactive red solution with an initial concentration of 10 mg L^{-1}. 15 mg of photocatalyst was added to each test tube. The solid–liquid mixture was magnetically stirred in the dark for 30 min to bring the photocatalyst to adsorption–desorption equilibrium. Then the mixture was placed vertically under a 300 W xenon lamp equipped with an optical transmission filter ($\lambda = 365$ nm). 5 mL of the mixture was centrifuged at intervals of 20 min to separate the solid photocatalyst from the solution. The absorbance was measured using a spectrophotometer (TU-1901) at the maximum absorption wavelength, 540 nm, of the reactive red solution, and the decolorization rate was calculated. The solution decolorization rate (D) was calculated via the following formula:

$$D = \frac{A_0 - A_t}{A_0} \times 100\% \qquad (1)$$

where A_0 represents the absorbance of the reactive red solution before illumination, and A_t represents the absorbance of the reactive red solution after irradiation.

3.   Results & discussion

X-ray diffraction patterns of the double-hybrid photocatalyst S, Nd–TiO₂ with different sulfur content are shown in Fig. 1. The S, Nd–TiO₂ samples show diffraction peaks at $2\theta = 25.2°$, 38.0°, 48.0°, 54.3°, 55.3°, 63.1°, 68.7°, 70.1°, and 74.9°, corresponding to the (101), (004), (200), (105), (211), (204), (116), (220), and (215) planes of anatase titania. These were confirmed to be from anatase titanium dioxide by comparison with JCPDS card #84-1286. In addition, the peaks at $2\theta = 27.0°$, 41.0°, 43.8°, and 56.6° can be ascribed to the (110), (111), (210), and (220) planes of a rutile titania structure. These were confirmed to be from rutile titanium dioxide by comparison with JCPDS card #75-1753. Fig. 1a shows the Nd–TiO₂ photocatalyst. This only shows anatase TiO₂ characteristics. Fig. 1b–d are double doped photocatalysts with different S doping amounts. The photocatalyst having a sulfur doping amount of 2% exhibited only anatase
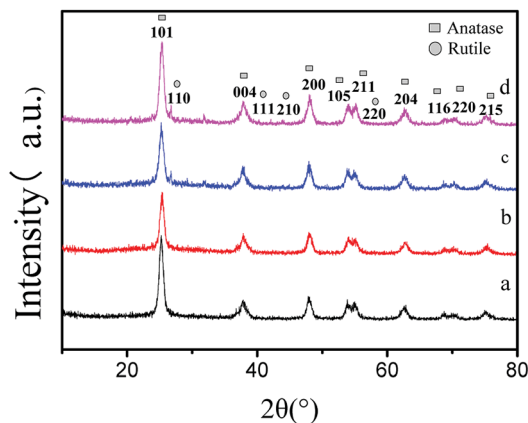
Fig. 1 XRD patterns of (a) Nd–TiO$_2$, (b) 2% S, Nd–TiO$_2$, (c) 4% S, Nd–TiO$_2$, and (d) 6% S, Nd–TiO$_2$.

Fig. 3 TEM images of (a) Nd–TiO$_2$, (b) 2% S, Nd–TiO$_2$, (c) 4% S, Nd–TiO$_2$, and (d) 6% S, Nd–TiO$_2$.

characteristics. The photocatalysts having sulfur doping amounts of 4% and 6% exhibited mixed crystal forms. In the experiment, we observed that with an increase in the amount of non-metallic sulfur doping, anatase type titanium dioxide gradually changed to rutile type. This may be due to the combined action of sulfur and neodymium to convert the photocatalyst to high stability rutile TiO$_2$. Although the doping of Nd can inhibit the crystalline phase transition of nano-TiO$_2$ and increase its thermal stability, an increase in the sulfur content will weaken the effects of neodymium. Because the band gap of the rutile phase is smaller than the forbidden bandwidth of the anatase phase, the absorption spectrum is red-shifted, and the response to visible light is enhanced. Therefore, the double-doped photocatalyst will have significantly higher degradability than the single-doped photocatalyst. The average grain size was calculated using the Scherrer formula: $D = k\lambda/\beta \cos\theta$ (D is the average grain size; k is a constant of 0.89; λ is the X-ray wavelength, equal to 0.154056 nm; β is the full width at half maximum; and θ is the diffraction angle). We can estimate the diameter of Nd–TiO$_2$ and S, Nd–TiO$_2$ particles. The average particle diameter of Nd–TiO$_2$ was 13.18 nm. 2% S, Nd–TiO$_2$ has a particle diameter of 17.66 nm, 4% S, Nd–TiO$_2$ has a particle diameter of 18.11 nm, and 6% S, Nd–TiO$_2$ has a particle diameter of 18.50 nm. It can be seen that Nd-doped TiO$_2$ shows reduced particle size, and the particle size of double-doped TiO$_2$ is less affected.

The particle size of pure TiO$_2$ is around 50 nm, but the doping of Nd leads to a decrease in TiO$_2$ grain size. An SEM
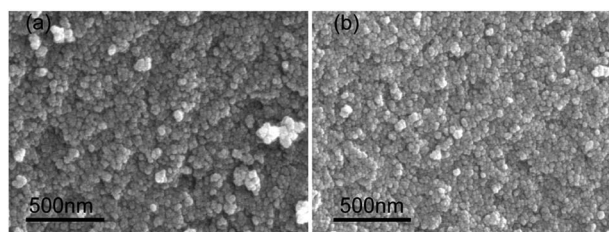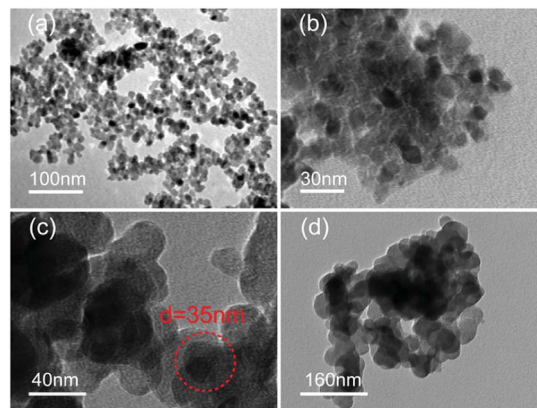

Fig. 2 SEM images of (a) Nd–TiO$_2$, and (b) S, Nd–TiO$_2$.

image in Fig. 2 shows as-prepared Nd–TiO$_2$ (Fig. 2a) with a size of about 15 nm. An SEM image in Fig. 2 also shows as-prepared S, Nd–TiO$_2$ (Fig. 2b) with a size of about 20 nm. The doped TiO$_2$ is spherical, which effectively reduces the issue of agglomeration and improves the dispersibility. The results show that both single and double doping can better improve the defects of TiO$_2$. Double-doped photocatalyst particles are significantly smaller in diameter than single-doped examples, which provides a basis for the better adsorption of dye molecules.

The TEM images in Fig. 3 show aggregated particles of Nd–TiO$_2$ (Fig. 3a) and S, Nd–TiO$_2$ (Fig. 3b–d), with particle sizes of 20 nm. In the Nd–TiO$_2$ and S, Nd–codoped-TiO$_2$ photocatalysts, the black Nd is more homogeneously dispersed in the TiO$_2$, which obviously improves the defect of TiO$_2$ agglomerating easily. Fig. 3b–d show double doped photocatalysts with different S concentrations. In Fig. 3c, the 4% S doped double doped photocatalyst disperses more evenly. Compared with the other photocatalysts, the doping of Nd and S has less effect on TiO$_2$, and all crystal grains are mainly spherical. The gap between crystal grains is homogeneous and the particle diameter is about 20 nm.

Fig. 4 shows XPS analysis of the S, Nd–TiO$_2$ photocatalyst. Since the photocatalytic activity of TiO$_2$ is affected by the type and content of doping elements, the chemical composition of S, Nd–TiO$_2$ is analyzed *via* XPS spectroscopy to detect whether S and Nd are co-doped into the TiO$_2$ lattice. The XPS spectrum shows that the photocatalyst S, Nd–TiO$_2$ is mainly composed of five elements: S, Nd, Ti, O and C. The Ti and O elements are derived from nano-titanium dioxide, the S and Nd elements are derived from the doping solution, and C is derived from organic precursor calcination residue. The binding energies of the Ti 2p1/2 peak and the Ti 2p3/2 peak are 464 eV and 457 eV, respectively; they differ by 7 eV, indicating that Ti is mainly present in the form of Ti^{4+}. The Ti 2p3/2 binding energy peak of pure TiO$_2$ is 459 eV. This indicates that the doping of TiO$_2$ by the two elements S and Nd causes the chemical environment of Ti to change, resulting in a chemical shift. 531 eV is a characteristic peak of a surface hydroxyl oxygen. This exists in the form of an Nd–O bond or Nd$_2$O$_3$ at 529 eV. The metal Nd has a large

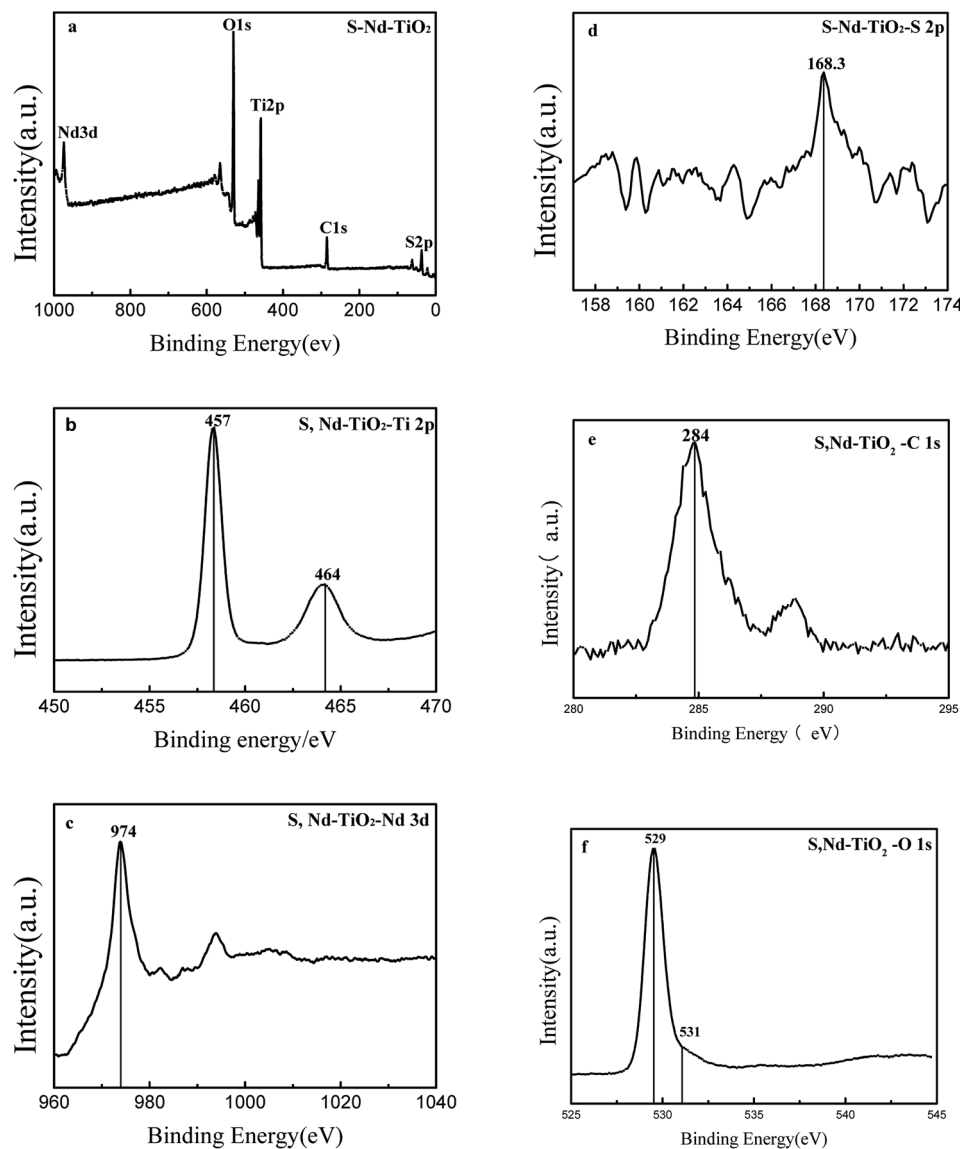Fig. 4   XPS spectra of (a) S, Nd−TiO₂: (b) the Ti 2p band, (c) the Nd 3d band, (d) the S 2p band, (e) the C 1s band, and (f) the O 1s band.

radius and is difficult to dope into TiO$_2$. Regarding the doping of sulfur, S 2p has a peak at 168 eV, indicating the doping of S in the TiO$_2$ lattice, possibly in the form of O–Ti–S. This is why S-doped TiO$_2$ has a visible light response. For S, Nd–TiO$_2$ particles, the binding energy of Nd 3d is located at 974 eV. In the S, Nd–TiO$_2$ photocatalyst, the Ti content is 19.53%, the O content is 53.01%, the Nd content is 1.08%, the S content is 0.12%, and the C content is 26.25%. Of these, carbon is mainly derived from the calcination of the photocatalyst, and the carbon content is too high due to the XPS analysis background. Therefore, we have reason to believe that Nd and S are successfully doped into the TiO$_2$ lattice.

Fig. 5 shows EDS spectra of the S, Nd-codoped-TiO$_2$ photocatalyst. Analyzing these, the four elements Ti, O, Nd and S are derived from the preparation of the photocatalyst, and the C element is derived from the calcination of the precursor. The results show that the element content is in the order of Ti > C > O > Nd > S, from high to low. It can be found from the test that

in the double-doped photocatalyst, the content of the sulfur element is significantly lower than that of the doping amount, and the content of the Nd element is level with the doping
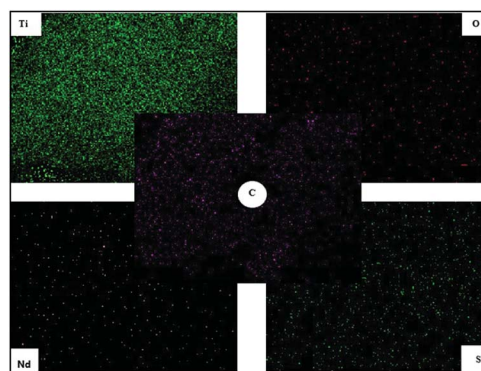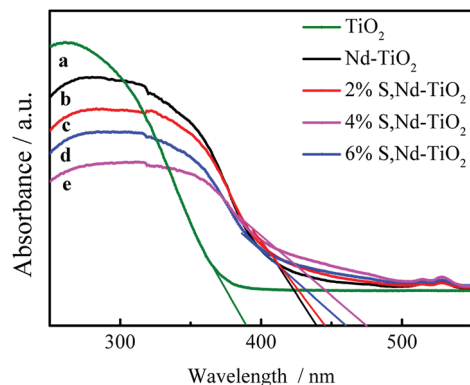

Fig. 5   EDS images of S, Nd−TiO₂.

Fig. 6 DRS spectra of single and double-doped photocatalysts: (a) TiO_2; (b) Nd–TiO_2; (c) 2% S, Nd–TiO_2; (d) 6% S, Nd–TiO_2; and (e) 4% S, Nd–TiO_2.

amount. This may be because Nd^{3+} is difficult to insert into the TiO_2 crystal lattice, and S^{6+} can replace Ti^{4+} in the TiO_2 crystal lattice, so the S element content detected by EDS and XPS is low.

DRS absorption spectra provided information about the wavelength region in which the catalyst absorbs light (Fig. 6). In the ultraviolet region, TiO_2 has the largest light absorption capabilities, which are significantly higher than those of the double-doped photocatalyst. The synthesized S, Nd–TiO_2 composites exhibited significantly stronger absorption compared to TiO_2 in the visible region. The synthesized 4% S, Nd–TiO_2 composite exhibited a clear absorption edge at approximately 476 nm in the visible light region, and a band gap energy of 2.61 eV was estimated *via* the equation: $\lambda_g = 1240/E_g$. Similarly, the forbidden band width of pure TiO_2 is 3.16 eV. In the infrared region, the four photocatalysts exhibited good light absorption capacity, and S, Nd double-doped photocatalysts showed significantly higher values than the single-doped photocatalyst. Pure TiO_2 can only absorb ultraviolet light, so the peak in the infrared region is caused by Nd doping. With an increase in S content, the peak increases correspondingly, indicating that S doping can promote the absorption of visible light by the photocatalyst. The experimental results show that the TiO_2 and Nd–TiO_2 calcined samples are white, while for the S, Nd–TiO_2 samples, as the S content increases, the light yellow color gradually deepens, which is consistent with corresponding literature reports.[26,27]

The nitrogen adsorption and desorption isotherms in Fig. 7 were used to characterize the structure of S, Nd–TiO_2. It shows a type V isotherm. S, Nd–TiO_2 shows a hysteresis loop at $P/P_0 = 0.45$–0.8, indicating that the new catalyst has mesopores, and there is no obvious inflexion point at $P/P_0 = 0.05$, which suggests that there are no micropores or very few micropores in the new material. From pore size distribution curve analysis, it is shown that the pore sizes of S, Nd–TiO_2 are mainly distributed between 30–50 nm, which is consistent with the TEM analysis results. The pore size of TiO_2 is between 50 and 90 nm, and the specific surface area is small. When S and Nd are doped into TiO_2, the pore size decreases and the pore volume decreases accordingly. The specific surface area was significantly higher than that of TiO_2, and the specific surface area was
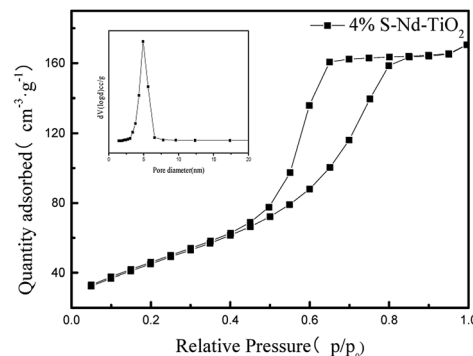

Fig. 7 The nitrogen adsorption–desorption isotherm and pore size distributions curve of 4% S, Nd–TiO_2.

about 3 times that of pure TiO_2. The specific surface area of the double-doped photocatalyst is 166.8 $m^2 g^{-1}$, and the specific surface area of pure TiO_2 is 56.5 $m^2 g^{-1}$. This shows that doping with Nd and S can suppress the lattice growth of TiO_2, increase the specific surface area, and increase the photocatalytic activity (Table 1).

Fig. 8 shows fluorescence spectra analysis of the semiconductor TiO_2 and the new catalysts. This was used to effectively investigate the recombination of electrons and holes on the surface of TiO_2 before and after modification. The results show that the fluorescence intensity of pure TiO_2 is large, and electrons and holes are easily recombined. With the doping of neodymium and sulfur, the fluorescence intensity of the composite decreases and the electron–hole recombination rate decreases. The doping of sulfur has no effect. The reason for this phenomenon is that the rare earth metal Nd forms a Ti–O–

Table 1 The specific surface area and pore size distribution parameters of TiO_2 and S, Nd–TiO_2

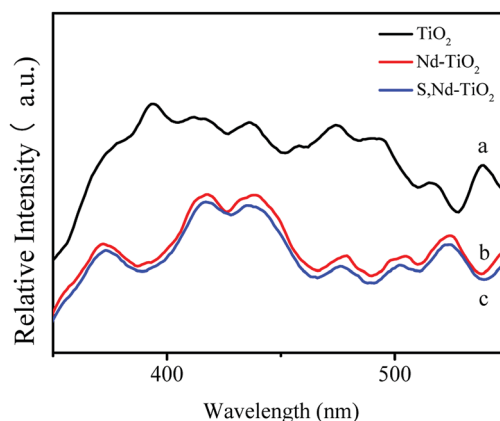| Sample	Surface area ($m^2 g^{-1}$)	Pore volume ($cm^3 g^{-1}$)	Crystallite size (nm)	P/P_0
TiO_2	56.50	0.9918	38.29	0.99915
S, Nd–TiO_2	166.82	0.2644	20.56	0.99578

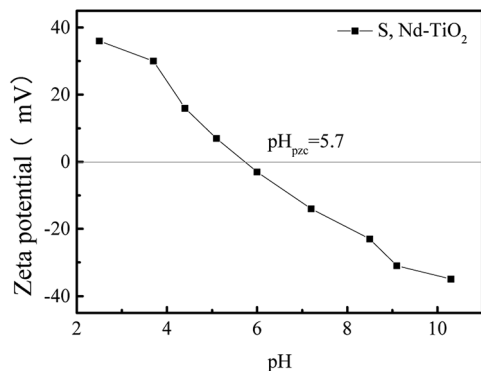**Fig. 8** PL fluorescence spectra analysis of each sample: (a) TiO_2; (b) Nd–TiO_2; and (c) S, Nd–TiO_2.

Fig. 9 The point of zero charge (pH_{pzc}) for the S, Nd–TiO$_2$ catalyst.

Nd bond around TiO$_2$. This is uniformly dispersed in the form of an oxide on the surface of TiO$_2$ or in the octahedral gaps of the TiO$_2$ lattice. In order to compensate for this charge imbalance, the surface of TiO$_2$ will adsorb more hydroxyl groups and promote the photocatalytic oxidation of TiO$_2$. This not only effectively separates photogenerated electrons and holes, but also generates more active hydroxyl groups, improving the photocatalytic performance of nano-TiO$_2$.

Fig. 9 shows the zeta potential values of S, Nd–TiO$_2$ photocatalysts under different pH conditions. The point at which the potential is zero is called the isoelectric point (pH_{pzc}). The adsorbent surface charge is neutral when pH = pH_{pzc}. The electrostatic force between the surface of the adsorbent and the ions is negligible. The double-doped photocatalyst S, Nd–TiO$_2$ has an isoelectric point of about 5.7. When the pH is less than 5.7, the zeta potential is greater than zero and the catalyst surface is positively charged. When the pH is greater than 5.7, the zeta potential is less than zero and the catalyst surface is negatively charged. Reactive red is an anionic dye, and the double-doped photocatalyst shows better adsorption effects due to electrostatic attraction.

4. Photocatalytic activity

4.1 Photocatalyst degradation tests

The photocatalytic activities of the S, Nd–TiO$_2$ nanocomposites were investigated by measuring the relationship between the degradation rate of reactive red solution irradiated by a xenon lamp and the irradiation time. In the degradation formula, C is the initial concentration of reactive red and C_t is the concentration after a fixed reaction time. The comparative experiment is degradation experiments conducted with the photocatalyst Nd–TiO$_2$. Stirring under dark conditions is indispensable prior to photocatalytic degradation. A quantitative amount of photocatalyst was added to the target degradant solution and magnetically stirred for 30 min to achieve adsorption and analytical equilibrium. For all samples, adsorption appeared to be of little use and the reactive red solution concentration did not change. But as the irradiation time increased, all samples degraded the reactive red solution. After 120 min using the single-doped photocatalyst, the degradation rate of reactive red

reached about 90%. Comparing the single-doped and double-doped photocatalysts, the double-doped photocatalysts have better abilities to degrade reactive red than the single-doped photocatalyst. So, the S doping described can significantly improve the catalyst activity. In addition, the photocatalytic activities of the single-doped photocatalyst Nd–TiO$_2$ and the double-doped photocatalyst S, Nd–TiO$_2$ were analyzed via the Langmuir–Hinshelwood kinetic model. The kinetic formula is as follows:

$$-\ln\frac{C_t}{C_0} = kt \qquad (2)$$

In the formula, C_0 is the initial concentration before the reactive red solution is degraded, and C_t is the concentration of the reactive red solution at different time points. The linear relationships between (C_t/C_0) and $-\ln(C_t/C_0)$ and the irradiation time are shown in Fig. 10 and 11. The rate constants of S, Nd–TiO$_2$ were higher than that of Nd–TiO$_2$. The above results indicated that 2% S, Nd–TiO$_2$, 4% S, Nd–TiO$_2$, and 6% S, Nd–TiO$_2$ exhibited higher photocatalytic activity than Nd–TiO$_2$. This is because Nd element doping prolongs the time of recombination of electrons and holes compared to pure TiO$_2$. Compared with Nd–TiO$_2$, the doping of S, Nd–TiO$_2$ broadens the light absorption range of nano-TiO$_2$. And 4% S, Nd–TiO$_2$ presented a slightly higher rate constant than 2% S, Nd–TiO$_2$ and 6% S, Nd–TiO$_2$. The degradation percentage of the reactive red solution by 4% S, Nd–TiO$_2$ photocatalyst after 160 minutes was 90.4%. The reactive red solution is almost completely decolorized, and the double-doped photocatalyst exhibits very high photocatalytic ability. The degradation rate of reactive red using Nd–TiO$_2$ was 0.0082 min^{-1}. The degradation rates of reactive red using 2% S, Nd–TiO$_2$ and 6% S, Nd–TiO$_2$ were 0.0131 min^{-1} and 0.0135 min^{-1}, respectively. Of the different samples, the 4% S, Nd–TiO$_2$ photocatalyst had the highest degradation rate towards reactive red solution, 0.0169 min^{-1}. The rate constants of the S, Nd–TiO$_2$ nanocomposites were higher than that of Nd–TiO$_2$ (0.0082 min^{-1}). The above results indicate that 2% S, Nd–TiO$_2$, 4% S, Nd–TiO$_2$ and 6% S, Nd–TiO$_2$ exhibited higher photocatalytic activity than Nd–TiO$_2$, which should be attributed to their bigger light absorption ranges and excellent adsorption performances. And 4% S, Nd–TiO$_2$ presented
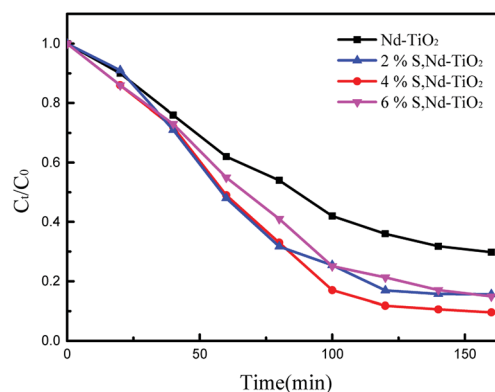

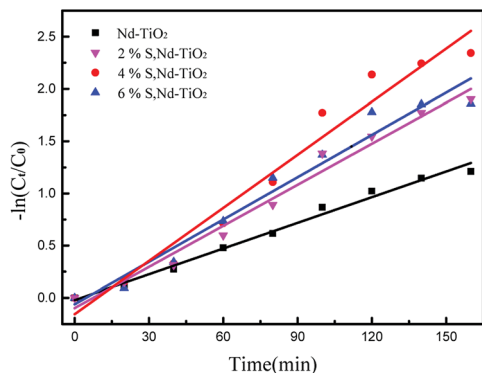**Fig. 10** Photocatalytic degradation of reactive red over S, Nd–TiO$_2$.

Fig. 11 Plots of $-\ln(C_t/C_0)$ *versus* irradiation time for the degradation of reactive red solution over S, Nd–TiO$_2$.

Fig. 12 The photocatalytic degradation of reactive red solution by S, Nd-codoped-TiO$_2$ under different pH conditions.

Fig. 13 Photocatalyst reusability efficiency.

a slightly higher rate constant than 2% S, Nd–TiO$_2$ and 6% S, Nd–TiO$_2$. In experiments, we chose the optimal doping amount of Nd as a basic quantity. The doping of different S content values (2%, 4% and 6%) widens the light absorption range of TiO$_2$. Too little S cannot modify TiO$_2$ very well, and too much S cannot enter the lattice of TiO$_2$, so 4% S, Nd–TiO$_2$ has the best photocatalytic efficiency.

4.2 Effect of pH on the degradation rates of the catalysts

Whether C_{H^+} in solution affects photocatalytic experiments is a problem we must consider. So, we conducted photocatalytic tests at different pH values. We chose 4% S, Nd–TiO$_2$ as a photocatalyst to perform pH tests. After the catalyst was added to solution, the pH of the solution was adjusted to 2, 4, 6, 8, or 10. After a certain amount of reactive red solution was sampled every 20 minutes, the absorbance was measured, and the degradation rate was calculated. We conclude that the double-doped photocatalyst has a wide pH response range, and the catalyst has the best degradation efficiency at pH = 4. Under acidic conditions, the catalyst can better absorb dye molecules on the surface. In the presence of hydroxyl radicals and the presence of suitable amounts of H$^+$, the reactive red (X-3B) molecule is eventually decomposed into small groups (NO$_3^-$, N$_2$, H$_2$O, CO$_2$, *etc.*). When it is exposed to light, the catalyst shows good ability to degrade reactive red. Under alkaline conditions, the reactive red dye molecules cannot be stably present, so the degradation rates of the catalysts are low. However, when the solution is alkaline, the double-doped photocatalysts still show more than 65% degradation. Therefore, the double-doped photocatalyst will have a wider pH response range and higher application value.

4.3 Photocatalytic repetition experiments

The multiple use of photocatalysts is important for practical value. Photocatalysts that retain their photocatalytic abilities after repeated degradation experiments are extremely rare. In this experiment, after the end of the first photocatalysis experiment, the upper liquid was poured out and the lower solid catalyst was collected and dried. The photocatalyst was replenished before the next photocatalytic experiment, so that
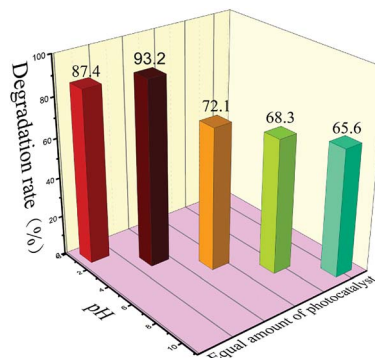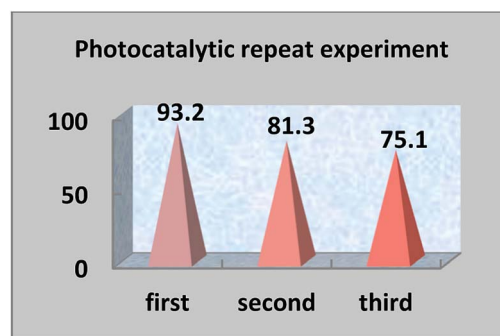
the photocatalytic experiment was carried out with the same amount of photocatalysts. Under the same light degradation conditions, the same concentration of reactive red solution was degraded again, and the degradation rate was calculated again. The photocatalytic degradation experiment was repeated three times to judge the reusability. In the experiment, we found that the photocatalyst S, Nd–TiO$_2$ has good reusability. As the photocatalyst is reused, the photocatalytic efficiency is lowered. The first cycle photocatalytic degradation amount reached 93%, the second cycle photocatalytic degradation amount reached 81%, and the third cycle photocatalytic degradation amount reached 75%. From the above results, it is shown that the double-doped photocatalyst S, Nd–TiO$_2$ has a high practical reusability value in active red solution (Fig. 12 and 13).

4.4 Photocatalytic mechanism

It is well known that the electron and hole recombination times determine the photocatalytic activities of catalysts, and the doping of Nd can effectively prolong the recombination time. The doping of an S element can effectively broaden the TiO$_2$ light absorption range and move this to the visible light region. Therefore, the S, Nd–TiO$_2$ double-doped photocatalyst combines the above advantages and exhibits excellent photocatalytic activity through testing. In the experiments, photocatalysis produces a large number of hydroxyl radicals, which can decompose organic matter into small molecules. The decomposed small molecule products of reactive red solution
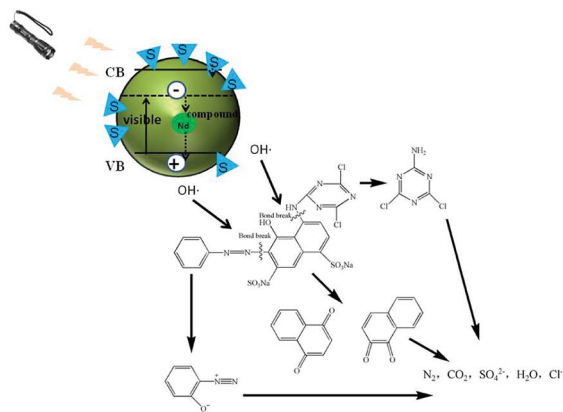
Fig. 14 Photocatalytic mechanism diagram.

after illumination are shown in Fig. 14. This coincides with the principle of hydroxyl radical degradation of organic matter reported in a large amount of literature. Single-doped photocatalysts still have limitations regarding the degradation of dyes and need improvement. Double-doped photocatalysts combine the two advantages and ultimately decompose the dye molecules into CO_2 and H_2O. This composite material has successfully improved the defects of TiO_2, and the low-consumption method has allowed the degradation of a practical dye solution, which provides a certain forward-looking route for real industry applications.

5. Conclusions

S, Nd-codoped-TiO_2 was prepared via a sol–gel method. The results of catalyst characterization show that the double-doped photocatalyst can effectively broaden the photoresponse range of TiO_2. From the EDS and XPS results, Nd and S were successfully doped into TiO_2. The S, Nd-codoped-TiO_2 photocatalyst has a large specific surface area: $S_{BET} = 166.82$ m^2 g^{-1}. Compared with many studies, our synthesized double-doped photocatalysts have higher degradation efficiencies.[28–30] The new photocatalysts improve the dispersibility of TiO_2 and enhance its characteristics regarding ease of agglomeration. The degradation results show that the photodegradation of reactive red solution reached 93.2% within 160 min using the S, Nd co-doped photocatalyst. The degradation of reactive red solution using Nd–TiO_2 after 160 minutes was 70%. The double-doped photocatalysts have significantly higher degradation abilities than the single-doped photocatalyst. The reason is that the doping of S and Nd not only broadens the light absorption range of TiO_2, but also reduces the recombination rate of electrons and holes. And the new photocatalyst has high stability and reusability. The double-doped photocatalyst is a promising photocatalytic material, which provides a great approach for solving water pollution issues with low consumption and high efficiency.

Conflicts of interest

There are no conflicts to declare.

Acknowledgements

Notes and references

1 S. Zong, W. Wei, H. Cui, Z. Jiang, X. Lü, M. Zhang and J. Xie, *Mater. Res. Innovations*, 2015, **19**, 361–367.

2 T. Ochiai, T. Fukuda, K. Nakata, T. Murakami, D. A. Tryk, Y. Koide and A. Fujishima, *Appl. Electrochem.*, 2010, **40**, 1737–1742.

3 M. S. Dieckmann and K. A. Gray, *Water Res.*, 2016, **30**, 1169–1183.

4 D. González, E. Cueto, F. Chinesta, P. Díez and A. Huerta, *J. Phys. Chem. C*, 2016, **117**, 1955–1962.

5 Z. Zhu, H. Pan, M. Murugananthan, J. Gong and Y. Zhang, *Appl. Catal., B*, 2018, **232**, 19–25.

6 H. K. Seo, C. M. Elliott and S. G. Ansari, *J. Nanosci. Nanotechnol.*, 2012, **12**, 6996–7001.

7 H. Barndõk, D. Hermosilla, L. Cortijo, C. Negro and Á. Blanco, *J. Adv. Oxid. Technol.*, 2016, **15**, 125–132.

8 J. Keleher, J. Bashant, N. Heldt, L. Johnson and Y. Li, *World J. Microbiol. Biotechnol.*, 2002, **18**, 133–139.

9 A. Fujishima and K. Honda, *Nature*, 1972, **238**, 37–38.

10 U. Diebold, *Surf. Sci. Rep.*, 2003, **48**, 53–229.

11 K. M. Reza, A. Kurny and F. Gulshan, *Appl. Water Sci.*, 2017, **7**, 1569–1578.

12 S. Garcia-Segura and E. Brillas, *J. Photochem. Photobiol., C*, 2017, **31**, 1–35.

13 V. Binas, D. Venieri, D. Kotzias and G. Kiriakidis, *Journal of Materiomics*, 2017, **3**, 3–16.

14 D. Zhao and C. F. Yang, *Renewable Sustainable Energy Rev.*, 2016, **54**, 1048–1059.

15 L. Hu, G. Zeng, G. Chen, H. Dong, Y. Liu, J. Wan, A. Chen, Z. Guo, M. Yan, H. Wu and Z. Yu, *J. Hazard. Mater.*, 2016, **301**, 106–118.

16 M. Reli, P. Huo, M. Šihor, N. Ambrožová, I. Troppová, L. Matějová, J. Lang, L. Svoboda, P. Kuśtrowski, M. Ritz, P. Praus and K. Kočí, *J. Sol-Gel Sci. Technol.*, 2017, **43**, 8564–8573.

17 S. Demirc, T. Dikici, M. Yurddaskal, S. Gultekin, M. Toparli and E. Celik, *Appl. Surf. Sci.*, 2016, **390**, 591–601.

18 W. Yan, S. M. Mahurin, Z. Pan, S. H. Overbury and S. Dai, *J. Am. Chem. Soc.*, 2005, **127**, 10480–10481.

19 Z. Xu and J. Yu, *Nanoscale*, 2011, **3**, 3138–3144.

20 C. Wang, L. Yin, L. Zhang, N. Liu, N. Lun and Y. Qi, *ACS Appl. Mater. Interfaces*, 2010, **2**, 3373–3377.

21 B. Trujillo-Navarrete, M. del Pilar Haro-Vázquez, R. María Félix-Navarro, F. Paraguay-Delgado, H. Alvarez-Huerta, S. Pérez-Sicairos and E. Alonso Reynoso-Soto, *Journal of Rare Earths*, 2017, **35**, 259–270.

22 T. Boningari, S. N. R. Inturi, M. Suidan and P. G. Smirniotis, *Chem. Eng. J.*, 2018, **339**, 249–258.

23 A. Charanpahari, S. S. Umare, S. P. Gokhale, V. Sudarsan, B. Sreedhar and R. Sasikala, *Appl. Catal., A*, 2012, **443–444**, 96–102.

24 A. Charanpahari, S. S. Umare and R. Sasikala, *Appl. Surf. Sci.*, 2013, **282**, 408–414.

25 F. Dong, H. Wang, G. Sen, Z. Wu and S. C. Lee, *J. Hazard. Mater.*, 2011, **187**, 509–516.

26 R. Asahi, T. Morikawa, T. Ohwaki, K. Aoki and Y. Taga, *Science*, 2001, **293**, 269–271.

27 Y. H. Xu, C. Chen, X. L. Yang, X. Li and B. F. Wang, *Appl. Surf. Sci.*, 2009, **255**, 8624–8628.

28 C. H. Cao, *Adv. Mater. Res.*, 2012, **488–489**, 221–225.

29 W. M. Hou and Y. Ku, *J. Alloys Compd.*, 2011, **509**, 5913–5918.

30 W. J. Zhang, M. L. Hu and H. B. He, *Adv. Mater. Res.*, 2012, **457–458**, 563–566.